European Journal of
Nuclear
Medicine

Original article

Effect of tissue heterogeneity on quantification in positron emission tomography

G. Blomqvist[1], A.A. Lammertsma[2], B. Mazoyer[3], K. Wienhard[4]

[1] Department of Clinical Neuroscience, Experimental Alcohol and Drug Addiction Research Section, Karolinska Hospital, Stockholm, Sweden
[2] PET Methodology Group, Cyclotron Unit, MRC Clinical Sciences Centre, Royal Postgraduate Medical School, Hammersmith Hospital, London, UK
[3] Service Hospitalier Frédéric Joliot CEA/Departement de Biologie, Hôpital d'Orsay and Antenne d'Informatique Médicale, Hôpital Robert Debré, Paris, France
[4] Max-Planck-Institut für Neurologische Forschung, Köln, Germany
Task Group of the Modelling Section of the EEC Concerted Action on PET Investigations of Cellular Regeneration and Degeneration

Received 14 December 1994 and in revised form 18 February 1995

Abstract. As a result of the limited spatial resolution of positron emission tomographic scanners, the measurements of physiological parameters are compromised by tissue heterogeneity. The effect of tissue heterogeneity on a number of parameters was studied by simulation and an analytical method. Five common tracer models were assessed. The input and tissue response functions were assumed to be free from noise and systematic errors. The kinetic model was assumed to be perfect. Two components with different kinetics were mixed in different proportions and contrast with respect to the model parameters. Different experimental protocols were investigated. Of three methods investigated for the measurement of cerebral blood flow (CBF) (steady state, dynamic, integral), the second one was least sensitive to errors caused by tissue heterogeneity and the main effect was an underestimation of the distribution volume. With the steady state method, errors in oxygen extraction fraction caused by tissue heterogeneity were always found to be less than the corresponding errors in CBF. For myocardial blood flow the steady state method was found to perform better than the bolus method. The net accumulation of substrate (i.e. $rCMR_{glc}$ in the case of glucose analogs) was found to be comparatively insensitive to tissue heterogeneity. Individual rate constants such as k_2 and k_3 for efflux and metabolism of the substrate in the pool of unmetabolized substrate in the tissue, respectively, were found to be more sensitive. In studies of radioligand binding, using only tracer doses, the effect of tissue heterogeneity on the parameter $k_{on} \cdot B_{max}$ could be considerable. In studies of radioligand binding using a protocol with two experiments, one with high and one with low specific activity, B_{max} was found to be insensitive while K_d was very sensitive to tissue heterogeneity.

Correspondence to: G. Blomqvist, Section of Clinical Neurophysiology, Karolinska Hospital, S-17176, Stockholm, Sweden

Key words: Positron emission tomography – Tissue heterogeneity – Tracer kinetics

Eur J Nucl Med (1995) 22:652–663

Introduction

The inherently limited spatial resolution of positron emission tomography (PET) and single-photon emission tomography (SPET) devices implies that, in general, more than one tissue component, each with a different physiological status, contribute to the measured signal in a volume element. Usually it is impossible to recover the signals from the different components. Therefore, the observed time-activity curve (TAC) of a tracer will be a mixture of the TACs of the components and, if the physiological parameters enter non-linearly in the model equations describing the time course, parameter estimates will not yield the mean values expected from linear mixing of the components.

In this report results obtained from investigations of the effect of tissue heterogeneity on a number of tracer procedures are presented: cerebral blood flow (CBF) and volume of distribution of water (V_d), myocardial blood flow (MBF), cerebral oxygen extraction fraction (OEF) and oxygen consumption ($CMRO_2$), cerebral metabolic rate of glucose (CMR_{glc}), and radioligand binding characteristics (B_{max}, k_{on}, k_{off}, K_d, $k_{on} \cdot B_{max}$).

Materials and methods

In this study the observed radioactivity concentration, $C_{mix}(t)$, is assumed to be a linear combination of two tissue components (e.g. grey and white matter) with concentrations $C_1(t)$ and $C_2(t)$ (radioactivity per unit volume):

$$C_{mix}(t)=f_1 \cdot C_1(t)+(1-f_1)\cdot C_2(t), \quad (1)$$

where f_1 is the fraction of component 1, a number between 0 and 1. Besides the assumption that only two components are present, it is assumed that the model is perfect for each tissue component, and also that the measurements are free from noise and systematic errors. Ideally, the parameter estimates should also be a linear combination, the true weighted mean p_{av}, of the parameter estimates for the components $p^{(1)}$ and $p^{(2)}$, respectively, with the same fraction:

$$p_{av}=f_1 \cdot p^{(1)}+(1-f_1)\cdot p^{(2)}. \quad (2)$$

This relation is valid when the parameters enter linearly in the model equation describing the theoretical TAC. This case can be illustrated by carbon-11 or oxygen-15 labelled CO, which are the most common tracers for the measurement of cerebral blood volume (CBV). As these tracers remain in the blood, the time course of the tissue radioactivity concentration $C(t)$ is well described by the following equation [1]:

$$C(t)=\mathrm{CBV}\cdot h \cdot C_{bl}(t), \quad (3)$$

where $C_{bl}(t)$ is the tracer concentration in the blood. (To correct for the different haematocrit values in cerebral and peripheral blood, a constant factor h is introduced.) If the measured tissue radioactivity concentration is a linear mixture of two components with different CBV values, the resulting CBV estimate will be the true mean of the CBV values of the components (f_1 is again the fraction of component 1):

$$C_{mix}(T)=f_1 \cdot C_1(t)+(1-f_1)\cdot C_2(t)=[f_1 \cdot \mathrm{CBV}_1+(1-f_1)\cdot \mathrm{CBV}_2]\cdot h \cdot C_{bl}(t). \quad (4)$$

This relation can be generalized to an arbitrary number of components. It should be noted that the true mean CBV is obtained as a factor in Eq. 4 because the factor $h \cdot C_{bl}(t)$ is common to all tissue components (provided the factor h is the same for all components). Similarly, the parameters K_{MR} (metabolic rate constant) and apparent distribution volume obtained in the Gjedde-Patlak analysis [2] enter linearly in the operational equation and are consequently insensitive to tissue heterogeneity.

In most models the expression for the TAC is non-linear in at least some of the unknown parameters. This is the case for compartmental models, where the time course of each of the partial concentrations is described by a differential equation. In such models the time course of the tracer is given by a (sum of) convolution integral(s) where unknown parameters enter non-linearly. As an example, in the model with only one compartment and no separate vascular volume, the tissue concentration at time T is given by the following expression:

$$C(T) = K_1 \cdot \int_0^T e^{[-k_2(T-t)]} C_{pl}(t)dt. \quad (5)$$

The tracer administration is assumed to start at T=0. K_1 and k_2 are the rate constants for forward and backward transport between blood/plasma and tissue and $C_{pl}(v)$ is the input function. In this expression the rate constant K_1 enters linearly and k_2 enters non-linearly. In the presence of tissue heterogeneity the non-linearity implies a deviation of the estimated parameters from the true average given by Eq. 2. It is even possible that the obtained parameter estimate, p_{mix}, falls outside the interval $[p^{(1)}, p^{(2)}]$. The tissue heterogeneity also affects the estimate of K_1, although this parameter enters linearly in the operational equation. This can be seen from the mixing (with fractions f_1 and $1\text{-}f_1$) of two tissue components described by different sets of (K_1, k_2) values:

$$C_{mix}(T) = f_1 C_1(T) + (1-f_1)C_2(T) = f_1 \cdot K_1^{(1)} \cdot \int_0^T e^{[-k_2^{(1)}(T-t)]} C_{pl}(t)dt + (1-f_1)\cdot K_1^{(2)} \cdot \int_0^T e^{[-k_2^{(2)}(T-t)]} C_{pl}(t)dt. \quad (6)$$

In contrast to the mean CBV in Eq. 4, the true mean of the K_1 values, $f_1 \cdot K_1^{(1)}+(1\text{-}f_1)K_1^{(2)}$, does not enter as a factor in Eq. 6. This indicates that tissue heterogeneity also affects parameters which enter linearly (like K_1), as soon as there is at least one parameter (like k_2) that enters non-linearly in the model expression. Only when k_2 is the same for all tissue components does the true mean become a factor in Eq. 6. Thus, in this case, the heterogeneity effects depend on the contrast in k_2 between the mixed tissue components.

Analytical method

The effects of tissue heterogeneity can be studied either analytically or by simulation studies. The "analytical method" [3] is based on Taylor expansion of the expression for the tracer radioactivity around the weighted mean values of the parameters, and can be used for models which give the tissue radioactivity as an explicit function of the model parameters. This is, for instance, the case when the differential equations governing the time course of the tracer are linear with constant coefficients. An example is given by Eq. 4 above. Another example is the solution to the frequently used tracer model with two tissue compartments, one of which is irreversible:

$$C(T) = p_0 \cdot C_{bl}(T) + p_1 \int_0^T e^{[-p_2(T-t)]} C_{pl}(t)dt + p_3 \int_0^T C_{pl}(t)dt,$$

$$\text{where } p_0 = \mathrm{CBV}, p_1 = \frac{K_1 \cdot k_2}{k_2 + k_3}, p_2 = k_2 + k_3, \text{and } p_3 = \frac{K_1 \cdot k_3}{(k_2 + k_3)}. \quad (7)$$

A different convention is to mulitply p_1 and p_3 by a factor ($1\text{-}V_f$), where V_f is the vascular fraction, a dimensionless number between 0 and 1. With this alternative convention the concentration of tracer in tissue is measured with respect to the tissue volume, i.e. the remaining volume after subtraction of the vascular volume. In this report we follow the convention used in Eq. 7, i.e. the concentration of tracer in tissue is measured with respect to the total volume with the vascular volume included. As the vascular volume is small in most cases considered, the two conventions give only slightly different concentrations in the tissue compartments.

In deriving the analytic method it was assumed that differences between fitted and true weighted average parameters are small and, therefore, second- and higher-order terms in the Taylor series expansion were neglected in [3]. In the following we assume a 10%–15% deviation of the fitted parameter value from the true average to be small enough to justify use of the analytical method.

Expressions for the deviation of a fitted parameter from the true mean (Eq. 2) have been presented in [3]. For example, the deviation $\Delta p_3=(p_3)_{fit}-(p_3)_{av}$, between the estimated value and weighted true mean of parameter p_3, can be expressed as (Eq. 24a in [3]):

$$\Delta p_3=(p_1)_{av}\cdot \varepsilon_3((p_2)_{av}\cdot \Delta T)\cdot \nu_3^2. \quad (8)$$

Besides $(p_2)_{av}$ scaled by the total measuring time, ΔT, the function ε_3 depends on the shape of the input function C_{pl}. The dependence of the degree of heterogeneity effects on the parameter p_2 is expected. If p_2 were the same for all tissue components, the operational equation should be linear in all parameters, and no heterogeneity effects should be present (cf. the comments after Eq. 6). Graphs of the ε_3-function for different conditions are given in [3]. ν_3^2 is the relative variance of p_3 for different fractions f_1 of tissue 1 (Eq. 27a in [3]):

$$\nu_3^2 = \frac{\left[f_1 \cdot (p_3^{(1)} - (p_3)_{av})^2 + (1-f_1)\cdot (p_3^{(2)} - (p_3)_{av})^2\right]}{(p_3)_{av}^2}, \quad (9)$$

where $p_3^{(1)}$, $p_3^{(2)}$ are the values of p_3 for tissue components 1 and 2, respectively. The errors of the parameters in different compartmental configurations can be treated analogously. In the same paper it was also shown that non-linear effects are present not only for parameters that enter non-linearly, but also for parameters that enter linearly in the theoretical expressions for the TACs. Only when *all* parameters enter linearly in these expressions, as in Eq. 3, are the non-linear effects absent. These features of non-linear model equations are illustrated by Eqs. 4 and 6 above.

Simulations

If more complicated differential equations are needed to describe the time course of the tracer, e.g. when radioligands with low specific activity are studied, an explicit solution of the equations may not be obtainable. In this case simulation studies are necessary. With this method tissue uptake curves, each determined by a given input function and a certain set of parameter values, are generated numerically by computer. The uptake curves are given either as an explicit expression in the parameters and the input function, or by the differential equations describing the time course of the tracer. In the latter case the equations have to be solved numerically. In the former case the solutions are often expressed as convolutions of the input function (cf. Eqs. 5 and 7). If the input function has a simple mathematical form these convolutions can be described by explicit expressions in the parameter values, otherwise they have to be calculated numerically. Linear combinations of two of the uptake curves, C_{mix} (Eq. 1), are formed with prescribed proportions of each tissue component.

The kinetic model is fitted to the generated mixed uptake curve $C_{mix}(t)$ under the assumption that only one component contributes. Parameter estimates were obtained by minimizing an unweighted sum of squared residuals using standard algorithms: the Marquardt algorithm using the RFIT package [4], a Gauss-Newton algorithm [5] or Davidon-Fletchers alternating gradient method using the MINUIT-routines [6]. In practice the terms in the sum of squared residuals are often weighted with the (estimated) random errors of the measurements. The effect of random measurement errors (i.e. noise) is not treated in this report, which is the reason why unweighted terms are used in the sum of squared residuals.

The resulting parameter estimates are compared to the true weighted mean values, p_{av}, expected from the linear mixing of components (Eq. 2). The differences Δp between parameter values expected from the linear mixing and the values actually obtained in the fitting process are analysed as a function of the mixing fraction and as a function of the contrast between the parameter values of the two components, i.e. as a function of the ratio between the kinetic parameter values $(p_i^{(1)}/p_i^{(2)})$ for describing the two components.

Five compartmental configurations that cover most of the tracer kinetic methods presently in use have been considered in this investigation. The kinetic models and the experimental protocols which have been analysed or simulated are summarized in Table 1. In the same table the different parameter settings are also given, together with details of the algorithm used in the parameter fit.

One single compartment

This configuration applies to freely diffusible tracers used in studies of CBF. Steady state [7], dynamic [8] and integral (or "autoradiographic") [9] methods using inhalation of $[^{15}O]CO_2$ or intravenous injection of $[^{15}O]H_2O$ were assessed. For the *steady state method* the calculations of the tissue concentration were based on the steady state equation given in [7] with the usual assumption that V_d=1. Different values of CBF were used. For the *dynamic method* TACs were generated over a measuring time of 3 min. The time course of the tracer is described by Eq. 5 (if only one component is present). Three different input functions were used: 2 min inhalation of $[^{15}O]CO_2$, 1 min infusion of $[^{15}O]H_2O$ and bolus injection of $[^{15}O]H_2O$. The resulting average tissue TACs were fitted for CBF and V_d. For the *integral method* the same input functions were used as for the dynamic method. The total tissue activity over the integration period was calculated. Integration periods for the slow input functions (inhalation and infusion) were identical to the administration intervals, i.e. 2 min for the inhalation and 1 min for the infusion protocols. For the bolus injection method the typical integral period of 40 s [10] was used. In the calculation of average CBF a V_d of 0.95 ml/ml was used.

A number of combinations of grey and white matter CBF and V_d were analysed. Reduced (0.2 ml/ml/min), normal (0.8 ml/ml/min) and increased (1.6 ml/ml/min) grey matter CBF values were used with a normal grey matter V_d of 1.02 ml/ml. Reduced grey matter CBF was also combined with a reduced V_d of 0.2 ml/ml. For most cases normal white matter CBF (0.2 ml/ml/min) and V_d (0.88 ml/ml) were used. However, in cases where grey matter CBF was reduced, a reduced white matter CBF (0.05 ml/ml/min) was also included in the analysis with and without reduction in white matter V_d (0.2 ml/ml). The effect of tissue heterogeneity in tumor tissue has been investigated separately [11].

One tissue compartment

This configuration is used when a distinction between the TACs in the vascular volume and the tissue is necessary, e.g. in studies of MBF and in studies of the transport across the blood-brain barrier using tracers that are not freely diffusible and enter only one pool in the tissue (i.e. no metabolism, no binding).

MBF using $[^{15}O]H_2O$ and $[^{15}O]CO_2$. In the first approximation the normal myocardium can be considered as homogeneous with respect to perfusion. However, when considering a region of interest (ROI) drawn on the myocardium in a tomographic slice, one can imagine at least two phenomena leading to tissue heterogeneity. First, due to the limited spatial resolution of current PET scanners, spill-over from right and/or left cavities and lung tissue into the myocardium cannot be neglected. Second, due to limited counting statistics available in human studies, heart data are seldom acquired with ECG gating. The heart motion is therefore likely to contribute a certain degree of tissue heterogeneity.

Concerning studies of MBF using $[^{15}O]H_2O$, three typical situations can be distinguished:

1. Spill-over from left cavity (LV) and lung (LU), such as is encountered when analysing lateral wall regions. The lung signal is predominantly vascular and can therefore be operationally confounded with the left cavity spill-over signal. The more complicated situation when the LV signal is different from the LU signal is not treated. Consequently, this situation consists of a single tissue compartment with spill-over from the arterial input compartment. Exchange of water between arterial blood and homogeneous tissue is supposed to be adequately described by a single tissue compartment model. The spill-over fraction is usually accounted for either by subtracting blood pool scans from the $[^{15}O]H_2O$ uptake

Table 1. Summary of the tracer models and experimental protocols

Physiological parameters	Simulated tracer	Kinetic model, model parameters	Details of algorithm	Analytic method	Simulated experimental protocol	Parameter settings in simulated data
CBF	$[^{15}O]CO_2$	Single compartment; CBF model	V_d=1 in the fit	Simulation	Inhalation; steady state	$CBF^{(1)}$=0.2, 0.8, 1.6 $CBF^{(2)}$=0.05, 0.2
		Single compartment; CBF model	V_d=1 in the fit	Simulation	Inhalation 2 min; 3-min dyn. scan	
CBF, V_d	$[^{15}O]H_2O$	single compartment; CBF model		Simulation	Bolus/1 min infusion; 3-min dyn. scan	$V_d^{(1)}$=0.2, 1.02 $V_d^{(2)}$=0.88
CBF		Single compartment; CBF model	V_d=0.95 in the fit	Simulation	Bolus/inhalation/slow infusion; 3-min scan autoradiographic	
MBF	$[^{15}O]H_2O$	One tissue compartment; K_1, k_2, V_f	MBF from K_1; V_f fitted	Simulation	Bolus; 5-min dyn. scan	a) *Lateral wall:* fit PET data b) *Septum, LV and RV spill-over:*
	$[^{15}O]H_2O$	One tissue compartment; K_1, k_2	V_f from $[^{11}C]CO$; MBF from k_2	Simulation	Bolus; 5-min dyn. scan	K_1=0.2, 0.5, 1.2, 5 p=0.2, 0.5, 1 $f_{LV}=f_{RV}$=5%, 10%, 20%, 30%, 45%
	$[^{15}O]CO_2$	One tissue compartment; K_1, k_2, V_f	MBF from K_1; V_f fitted	Simulation	Inhalation; 6.5-min dyn. scan; fit of vascular fraction	c)*Heterogenity, high and low flow tissue mixing:* $K_1^{(1)}$=1, 2, 5 $V_d^{(1)}$=1 $K_1^{(2)}$=0.2, 0.5, 1.2 $V_d^{(2)}$=1, 0.5 f_l=25%, 50%, 75% V_l=10%
Influx across BBB	[^{11}C]methyl-glucose	One tissue compartment; K_1, k_2		Analytic	Bolus; 40-min scan	$k_2^{(1)}:k_2^{(2)}$=2:1
$CMRO_2$ OEF, CBF	$[^{15}O]O_2$	$CMRO_2$ model		Simulation	Inhalation; steady state	CBV=0.02, 0.05; OEF=0.1, 0.4, 0.9 $CBF^{(1)}$=0.2, 0.8, 1.6; $CBF^{(2)}$=0.05, 0.2 $V_d^{(1)}$=0.2, 1.02; $V_d^{(2)}$=0.88 $OEF^{(1)}$ $OEF^{(2)}$
CMR_{glc}, influx across BBB	FDG	Two tissue compartments; K_1, k_2, k_3, k_4	k_4=0 in the fit	Analytic	Bolus; 40-min scan	$(k_2+k_3)^{(1)}:(k_2+k_3)^{(2)}$= 2:1 $(k_2+k_3)^{(1)}:(k_2+k_3)^{(2)}$= 4:1 $(k_2+k_3)^{(1)}:(k_2+k_3)^{(2)}$=10:1
MAO-B activity (k_3)	[^{11}C]deprenyl	Two tissue compartments; K_1, k_2, k_3, V_f	Fit of blood volume	Simulation	30-min scan	$K_1^{(1)}$=0.7, $k_2^{(1)}$=0.2, $k_3^{(1)}$=0.25, $V_f^{(1)}$=0.07 $K_1^{(2)}$=0.2, $k_2^{(2)}$=0.06, 0.2, $k_3^{(2)}$=0.1, 0.25, $V_f^{(2)}$=0.02
Receptor density	FESP	Two tissue compartments; K_1, k_2, k_3, k_4; $k_3=k_{on}\cdot B_{max}$	$k_4\neq0$ alt. k_4=0 in the fit	Simulation	Bolus; 180-min scan	$(k_1, k_2)^{(1)}=(K_1, k_2)^{(2)}$ $K_1^{(1)}$=0.28, $k_2^{(1)}$=0.073, k_3=0.075 $(k_1, k_2)^{(1)}\neq(K_1, k_2)^{(2)}$ $K_1^{(2)}$=0.07, $k_2^{(2)}$=0.03
Receptor density (B_{max}), equilibrium diss. rate, ass. and diss. rates	[^{11}C]fluma-zenil	Standard model radioligands; B_{max}, k_{on}, k_{off}, k_1, k_2	Num. solution	Simulation	Bolus; 2·60-min scans; high+low SA	B_{max}=120, k_{on}=0.004, k_{off}=0.05; K_{on}=0.40, k_{off}=0.50, $K_1^{(2)}$=0.10, 0.40; $k_2^{(2)}$=0.15, 0.50

Units: blood flow (CBF, TBF,MBF): ml blood/ml tissue/min; distribution volume (V_dv): ml blood/ml tissue; K_1:/min; k_2:/min; k_3:/min; k_4:/min; blood volume (CBV, V_f): ml blood/ml tissue (%); B_{max}: pmol/ml tissue; k_{on}: ml tiss·min/pmol; k_{off}: /min

curves or by including an extra term $f_s \cdot C_a(t)$, where $C_a(t)$ is the arterial input and f_s is the spill-over fraction. Consequently, this situation consists of a single tissue compartment with some spill-over from the arterial input compartment:

$$C_{mix}(T) = f_s \cdot C_a(T) + (1 - f_s) \cdot K_1 \cdot \int_0^T e^{[-k_2(T-t)]} C_a(t) dt. \quad (10)$$

2. Spill-over from both left and right ventricle cavities (LV and RV), which occurs when MBF is measured in septal regions. Because of delay and dispersion in the pulmonary circulation, LV and RV spill-overs cannot be combined into a single spill-over component and subsequently treated analogously to the spill-over fraction in the first situation. Moreover, the RV signal amplitude may be very large, especially during the first pass of the radioactive bolus in the right cavities, and can thus contribute significantly to septal ROI signals. This situation was simulated by adding various fractions (f_{LV} and f_{RV}) of the left ventricle [$C_{LV}(t)$] and right ventricle TACs [$C_{RV}(t)$] to the convolution expression in Eq. 4. Thus the ROI radioactivity concentration in this situation can be described by the following equation:

$$C_{mix}(t) = f_{LV} \cdot C_{LV}(t) + f_{RV} \cdot C_{RV}(t) + (1 - f_{LV} - f_{RV}) \cdot K_1 \cdot \int_0^T e^{[-k_2(T-t)]} C_{LV}(t) dt. \quad (11)$$

3. Mixing a myocardial tissue with different MBF and/or partition coefficients, which occurs, for example, when residual perfusion is measured in infarcted areas. This situation is very similar to that of the brain studies, and has been extensively discussed by Herholz and Patlak [3], with the exception of the existence of a significant vascular contribution. In the present study this situation was simulated by combining two myocardial uptake curves with varying fractions f_1 of tissue component 1 and with different parameter sets [$K_1^{(1)}$, $k_2^{(1)}$ and $K_1^{(2)}$, $k_2^{(2)}$ respectively]:

$$C_{mix}(T) = f_{VL} \cdot C_{LV}(T) + f_1 \cdot (1 - f_{VL}) \cdot K_1^{(1)} \cdot \int_0^T e^{[-k_2^{(1)}(T-t)]} C_{LV}(t) dt. + (1 - f_1)(1 - f_{VL}) \cdot K_1^{(2)} \cdot \int_0^T e^{[-k_2^{(2)}(T-t)]} C_{LV}(t) dt. \quad (12)$$

Two different ways of administrating the tracer were investigated: intravenous bolus injections of [^{15}O]H_2O [12, 13] and [^{15}O]CO_2 inhalation, according to the build-up washout protocol [14, 15]. The bolus and inhalation scanning protocols were 15×4 s followed by 24×10 s, and 15×4 s followed by 24×10 s followed by 3×30 s, respectively. In both implementations, the entire data set was taken into consideration in the fitting procedure. Thus three parameters were estimated: K_1 (ml blood/min/ml tissue), k_2 (/min) and a vascular fraction V_f (no unit).

Although rMBF is traditionally assumed to be estimated by the blood-to-brain transfer rate constant K_1 [16], the tissue heterogeneity effects on rMBF as measured by "Iida's method" [12] were also explored. In this latter approach, rMBF is supposed to be proportional to k_2 and the vascular contribution is either fitted or removed using a blood volume measurement using [^{15}O]CO. To simulate this situation, the arterial spill-over fraction was kept to a constant value equal to the sum of the LV and RV spill-over fractions that was used to generate the theoretical uptake curve. K_1 and RMBF(=k_2) were the fitted parameters. Input functions were assumed to be piecewise linear.

For the MBF studies LV, RV and LU TACs were obtained in a normal volunteer who underwent both a bolus of [^{15}O]H_2O and, 20 min later, a [^{15}O]CO_2 inhalation study. Data were acquired on the TTV03 time-of-flight positron tomograph [17]. The LV, RV and LU regions were drawn on the basis of fluorine-18 fluorodeoxyglucose ([^{18}F]FDG) scan acquired 40 min later.

[^{11}C]methylglucose. The glucose analog 3-0-[^{11}C]-methyl-D-glucose (MG) is not metabolized in the brain and the kinetics of this tracer are well described by a single-tissue compartment model with two rate constants K_1 and k_2 for transport in and out across the blood-brain barrier (BBB), respectively [18]. The CBV value was assumed to be known. Eq. 6 was used as the operational equation. The considerations by Herholz and Patlak regarding the CBF model were applied.

Oxygen consumption

Only the "steady state method" using continuous inhalation of [^{15}O]O_2 was assessed [7, 19], in a similar way to steady state CBF (see above). The same flow combinations were utilized with different combinations of OEF and CBV. Although the measurement of CBV is linearly related to measured [^{15}O]CO or [^{11}C]CO activity and thus is not itself affected by tissue heterogeneity, it is still important since the correction for intravascular activity in the steady state method is non-linear.

CBV values of 0.02 and 0.05 were used, and for normal and increased grey matter CBF an additional CBV value of 0.20. OEF values were assumed to be 0.1 or 0.4 in situations of increased CBF, and 0.4 or 0.9 for decreased CBF. For normal CBF all three different OEF values were tested. Simulations of abnormal OEF conditions were performed assuming paired changes in grey and white matter OEF or only a change in grey matter OEF with normal white matter OEF. Since $CMRO_2$ in a region (pixel) is basically obtained by multiplying the CBF and OEF values in the same region (pixel), it follows that the percentage error in $CMRO_2$ is the sum of the errors in both measurements.

Two tissue compartments

The exchange between the plasma and the free (unmetabolized or unbound) tracer in the tissue is described by the rate constants K_1 and k_2, while the exchange between the two tissue compartments (free and metabolized/bound, respectively) is described by the rate constants k_3 and k_4. If one of the tissue compartments is irreversible (k_4=0), Eq. 7 is the model equation for the total radioactivity concentration at time T. Examples of studies using this common configuration are glucose utilization using [^{18}F]FDG [20] and [1-^{11}C]-D-glucose [21], receptor binding using 3-*N*-[2'-^{18}F]fluoroethylspiperone (FESP) [22, 23], cerebral monoamine oxidase B activity (MAO-B) using [^{11}C]deprenyl [24] and amino acid utilization using [11C]methionine [25] or ^{18}F-tyrosine [26]. The effects of heterogeneity for two tracers, FDG and MAO-B, with low and high extraction fraction, respectively, were examined.

$rCMR_{glc}$ using FDG. The analytical method was applied (see above). The rate constant k_4 was put to zero, i.e. Eq. 7 was used as the model equation. For FDG a reasonable value of p_2 is k_2+k_3 is ≈0.2/min. With measuring time equal to 40 min this restricts the ε_3-function (Eq. 8) to values less than 0.1. By experience, even in extreme cases the ε_3-function is smaller than 0.2/min. The relative errors of the metabolic rate, $\Delta p_3/p_3$, depend linearly on $p_1/p_3=k_2/k_3$ (Eq. 8). This ratio was approximated by a fixed number, 3.

Cerebral monoamine oxidase B (MAO-B) activity using [^{11}C]deprenyl. For MAO-B a dynamic scanning protocol using bolus injection of [^{11}C]deprenyl and non-linear regression analysis for K_1, k_2, k_3 and V_f (effective blood volume) was assessed. For the assess-

ment of MAO-B activity, the behavior of k_3 is of particular interest. At present there is only limited experience with [^{11}C]deprenyl which suggests that k_3 and possibly k_2 are of the same order of magnitude in grey and white matter. In addition, due to the high extraction fraction, K_1 values are close to CBF values.

Standard model for radioligands

The aim of receptor studies with PET is to measure quantitatively the binding characteristics of radioligands (free receptor concentration B_{max}, association rate constant k_{on}, dissociation rate constant k_{off}, and equilibrium dissociation constant K_d=k_{off}/k_{on}) in distinct tissue regions. The "standard model" for radioligands [27] includes two compartments, one for free and one for specifically bound radioligand. The model has here been applied to studies using FESP and [^{11}C]flumazenil. Tissue heterogeneity effects may arise either from admixtures of tissue with different pharmacokinetics and receptor density or from contribution of tissue free from receptors.

Only tracer doses of radioligands: FESP. Like labelled spiperone and alkylated spiperone analogues such as methylspiperone or ethylspiperone, FESP binds essentially irreversibly to dopamine D2 receptors in the human striatum [23, 28–31]. The case of "tracer dose", when the unlabelled ligand does not affect the number of available binding sites, is considered here. A two tissue compartment model including rate constants K_1–k_4 is then applicable and specific binding is described by the rate constant k_3=k_{on}·B_{max}. If the binding is completely irreversible, k_{off} (here denoted k_4) is equal to zero. Transport from blood into tissue and back again together with rapid non-specific binding is lumped into rate constants K_1 and k_2. In receptor-free tissue (but with possible non-specific binding) the model reduces to a one tissue compartment model with k_3 and k_4 equal to zero. In such tissue the rate constants K_1 and k_2 can be similar to or largely different from those of the tissue with specific binding. This may simulate fits of non-zero k_4 even for a ligand with irreversible binding, which, in turn, may influence the fitted k_3 value. As the two tissue components are described by two different compartmental configurations, the heterogeneity effects were studied by simulations.

TACs were simulated using blood time-activity data and values of K_1, k_2 and k_3 from a previous patient study. Simulated data for tissue with specific, irreversible binding (i.e. with k_4=0) were mixed with data for tissue with no binding (k_3=k_4=0). Two cases were considered: (a) same K_1 and k_2 values for both components and (b) K_1 reduced by a factor of 4 and k_2 by a factor of 2 for the component void of receptors compared to the tissue with receptors, to simulate the tissue/blood partition coefficient in white matter of the patient study.

Pharmacological doses: [^{11}C]flumazenil. Only the kinetics of reversible ligands has been considered here. Non-specific, non-saturable binding has not been taken into account. To disentangle B_{max} and k_{on}, it is necessary to combine at least two experiments, one with a low and one with a high amount of unlabelled ligand co-injected with the radioligand. One experiment is assumed to be performed with a negligible amount of unlabelled ligand co-injected with the radioligand [tracer dose, high specific activity (SA)]. In this case the time course of the bound radioligand is, in the framework of the standard model, described by a two tissue compartment model with rate constants K_1–k_4 (see above). In the second experiment an appreciable amount of unlabelled ligand is assumed to be co-injected with the radioligand (low SA). In the standard model the time courses of the free and bound radioligand concentrations, $C_F(t)$ and $C_B(t)$ respectively, are determined by the following two differential equations:

$$\frac{dC_F(t)}{dt} = K_1 \cdot C_{pl}(t) - k_2 \cdot C_F(t) - k_{on} \cdot \left[B_{max} - \frac{C_B(t)}{SA} \right] \cdot C_F(t) + k_{off} \cdot C_B(t), \quad (13a)$$

$$\frac{dC_B(t)}{dt} = k_{on} \cdot \left[B_{max} - \frac{C_B(t)}{SA} \right] \cdot C_F(t) - k_{off} \cdot C_B(t). \quad (13b)$$

Here $C_{pl}(t)$ is the time course of the input function. Only the ideal case where the rate constants K_1 and k_2 are completely known was investigated. These parameters are supposed to be determined (a) from a "reference region" devoid of receptors or (b) from a third "protection experiment". In the latter case the injection of a tracer dose of radioligand is preceded by an injection of a large amount of unlabelled ligand that will block the receptors for the radioligand. A single tissue compartment model (see above) is assumed to be valid for the uptake curve in the reference region and from the protection experiment, respectively. For both methods it is assumed that K_1 and k_2 are unaffected by the concentration of cold ligand. In case (a) the extra assumption must be made that K_1 and k_2 are the same in the reference region and regions with receptors.

The non-linearity of the tracer equations in the standard model for radioligands precludes use of the analytical method to analyse tissue heterogeneity effects. For a given input function and given values of K_1, k_2, B_{max}, k_{on}, k_{off}, CBV and specific activity, the time-activity data were generated by a simulation program which solved the system of differential equations governing the concentrations of the free and bound tracer in the tissue numerically (fourth-order Runge-Kutta). The case with mixing of two components was considered, one with binding where the TAC is described by the standard model (Eqs. 13a and b) and another, the "background tissue", without binding (B_{max}=0) where the TAC is described by a single tissue compartment model (Eq. 5). Simulations where the two tissue components had equal or unequal kinetics across the BBB (K_1 and k_2) were performed. Treated here is an experimental protocol including two experiments on the same subject, one with a tracer dose and another with a large amount of unlabelled ligand (low SA). The used input function was composed of two parts: a steeply rising linear part in a short initial time interval, followed by a mono-exponential decrease over the remaining time interval (40 min).

The method which uses the TAC in the reference region, $C_{ref}(t)$, as a measure of $C_F(t)$ in regions with receptors [32] was not considered. This simple method eliminates the need to determine the input function and only Eq. 13b needs to be considered. However, even when K_1 and k_2 are the same in the reference region and in a region with receptors, the time courses of the free radioligand are different in these regions, because in the presence of receptors the free radioligand can either leave the tissue or bind to the receptors, whereas without receptors the free radioligand can only leave the tissue. The difference between $C_F(t)$ and $C_{ref}(t)$ is largest in the initial time interval after a bolus injection and, provided the transport kinetics across the BBB are the same in the regions considered, becomes small at late times when the free radioligand in the tissue and the blood approaches the equilibrium state. Thus, use of a reference region in this way adds an extra systematic error to errors caused by tissue heterogeneity. For the same reason the widely used method to estimate B_{max} and K_d from equilibrium data "Scatchard analysis" was not considered.

Results and discussion

Single compartment

CBF

As expected, of the three methods analysed (steady state, dynamic, integral), the steady state method is most sensitive to changes in V_d (Fig. 1a). Interestingly, the highest error in the present simulation studies (≈70%) was found for pure "grey" matter with reduced CBF (0.2 ml/ml/min) and V_d (0.2 ml/ml). With respect to tissue heterogeneity, the highest error was found for increased grey matter CBF (1.6 ml/ml/min) with normal white matter CBF, i.e. the highest ratio between flow values. Maximum underestimation of mean CBF was approximately 45% for a region containing 20%–30% grey matter.

With respect to errors in CBF due to tissue heterogeneity, best results were obtained with the dynamic method (Fig. 1b). In this case the maximum underestimation of mean CBF was ≈7%, again for the largest flow difference (1.6 vs 0.2 ml/ml/min). It is of interest to note that with this method, the main effect of tissue heterogeneity is an underestimation (up to around 40% for the condition given above) of V_d, as has been reported previously [33]. No significant difference between the three different tracer administration protocols was observed.

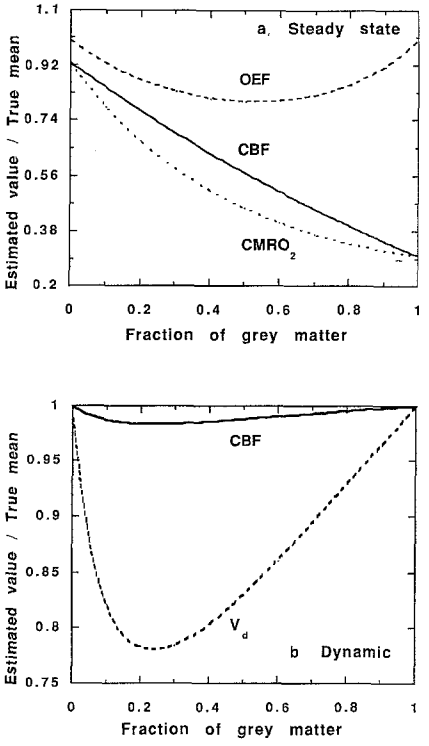

Fig. 1. a Effect of tissue heterogeneity on CBF (*solid line*). OEF (*dashed line*) and $CMRO_2$ (*dotted line*) calculated using the steady state method. The following parameter values for the two tissue components were used in the simulations (grey=component 1): $CBF^{(1)}$=0.2, $CBF^{(2)}$=0.2, $V_d^{(1)}$=0.2, $V_d^{(2)}$=0.88, $OEF^{(1)}$=0.9, $OEF^{(2)}$=0.4 $CBV^{(1)}$=0.05, $CBV^{(2)}$=0.02. The parameter setting corresponds to a situation with low grey $CBF/CMRO_2$ and normal white $CBF/CMRO_2$. **b** The effect of tissue heterogeneity on CBF (*solid line*) and V_d (*dashed line*). The "dynamic" method to calculate parameters was applied. The following parameter values for the two tissue components were used in the simulations: $CBF^{(1)}$=0.80, $CBF^{(2)}$=0.20, $V_d^{(1)}$=1.02, $V_d^{(2)}$=0.88. The parameter setting corresponds to mixing of normal grey and white matter

Results observed with the integral method showed the same pattern as that for the steady state method, although with smaller absolute errors. In addition, the shorter the integration period the better the performance with respect to tissue heterogeneity (in these cases where no noise was added to the data). The underestimation of pure (reduced) "grey" matter CBF (CBF=0.2 ml/ml/min, V_d=0.2 ml/ml) was 35%, 25% and 19% for 2 min, 1 min and 40 s, respectively. The maximum underestimation of mean CBF for the largest flow difference (1.6 vs 0.2 ml/ml/min) was now 25%, 18% and 14% for 2-min, 1-min and 40-s integration periods, respectively.

As for CBF, the highest observed error in tumor blood flow measured with the steady state technique, ≈70%, was not due to tissue heterogeneity, but due to V_d being substantially different from the assumed value of 1 ml/ml. It should be realized that this is a much more likely situation than in the bain. For the dynamic technique the error in tumor blood flow due to tissue heterogeneity was always small (<5%). Again, as for the brain, the major effect of tissue heterogeneity was an underestimation in V_d, which for the conditions simulated in the present study was 30% at maximum. Further results of simulation studies of this case are presented in [11].

One tissue compartment

MBF

Spill-over from lung and left ventricle. Figures 2a and b show the results for bolus and inhalation protocol respectively. Fitted parameters values were 0.06±0.01 ml/min/ml (K_1), 0.76±0.07 min (k_2) and 0.108±0.003 (f_s) for the bolus study, and 0.10±0.04 ml/min/ml (K_1), 1.0±0.3 min (k_2) and 0.107±0.014 (f_s) for the inhalation study. Note that the two implementations led to parameter estimates that were not significantly different. Adding delay and dispersion, parameters did not significantly improve the fits for either procedure. Because K_1 is quite small and k_2 quite large, the lung tissue contribution to the lung ROI activity is mainly due to blood radioactivity. As noted above, lung spill-over to lateral wall may be treated as additional blood spill-over in first approximation. However, it should be noted that the lung's apparent partition coefficient is very small (because of lung density). The consequences of this heterogeneity are of the same nature as that of situation (c) and will be detailed later.

Spill-over from both cavities into septum. Figure 3a depicts the effects of the right and left ventricle spill-over fraction on the rMBF value for the various model implementations. Notice the absence of proportionality be-

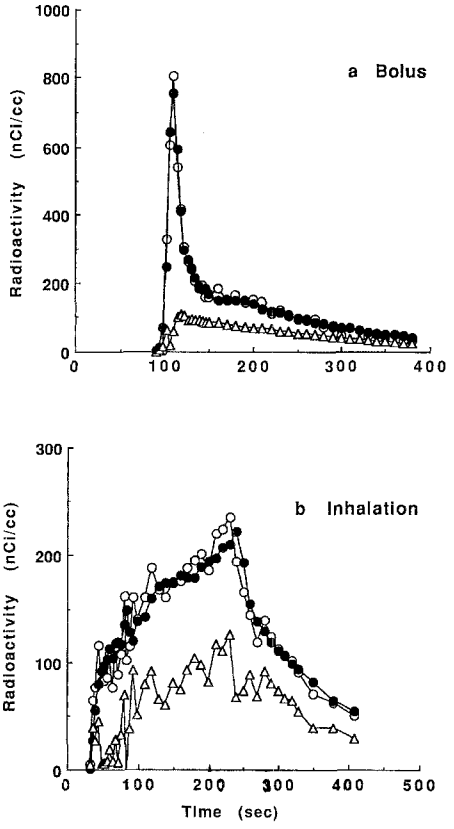

Fig. 2. Effects of spill-over from lung and left ventricle (**a**) bolus of $[^{15}O]H_2O$ and (**b**) inhalation of $[^{15}O]CO_2$. *Open circles*, lung ROI; *open triangles*, lung tissue (LU); *solid circles*, model fit. The time-activity curve from the left ventricle was used as input function and the LU component was calculated from the fitted parameters

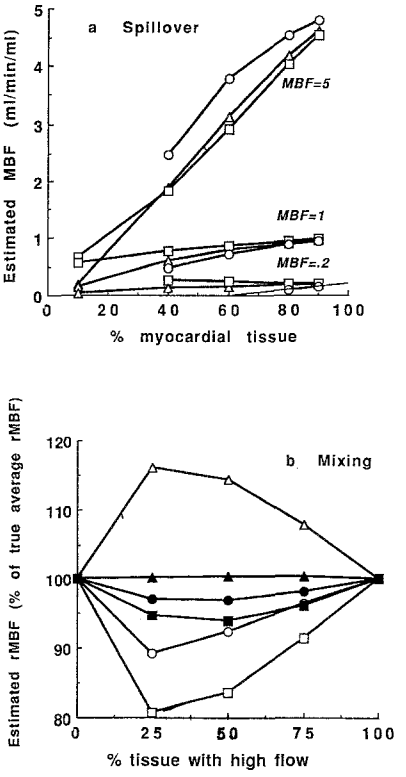

Fig. 3. a Changes in estimated MBF due to spill-over from the left and right cavities into a septal region. Different values of MBF (0.2, 1.0 and 5 ml/ml/min) have been considered. Three different methods of estimating MBF are compared. *Squares*, inhalation of $[^{15}O]CO_2$; *circles*, bolus injection of $[^{15}O]H_2O$; *triangles*, the method of Iida et al. (1988) for estimating MBF from k_2. **b** Change in estimated MBF due to mixing of tissue with different MBF. The high-flow component has MBF=1. The low-flow component has MBF=0.2 (*open symbols*), and MBF=0.5 (*solid symbols*), respectively. Three different methods of estimating MBF are compared. *Squares*, inhalation of $[^{15}O]CO_2$; *circles*, bolus injection of $[^{15}O]H_2O$; *triangles*, the method of Iida et al. (1988) for estimating MBF from k_2

tween tissue fraction and estimated MBF (except at very high flow). Note also that the inhalation protocol leads to estimated values closer to the true MBF. The explanation of this phenomenon is that, contrary to the brain situation, inclusion of a vascular fraction in the fit parameters allows the recovery of MBF values close to their true values. This performs better for inhalation than for bolus because the influence of the right ventricle spill-over is maximal for the bolus at early times, where RV activity arrives later in the inhalation protocol. In both implementations, the RV spill-over was taken into account by a larger vascular fraction. It performs not as well for Iida's method [12], where the vascular fraction is predefined at its true value. A possibility to overcome this drawback is to fit V_f [15].

Mixing of tissues with different MBF. It was observed that the larger the flow difference between the "low-flow" and "high-flow" components, the larger was the deviation from the true average (Fig. 3b). It was also observed that for a lower high-flow component, the deviation from the true average is smaller. It was also noted that Iida's implementation [12] was performing better than the other two methods, with the bolus implementation being superior to the inhalation method. Tissue heterogeneity was characterized by an underestimation of rMBF in all cases, except for Iida's method [12] when the flow differences were very large. However, Iida's method was sensitive to variation in the partition coefficient, a phenomenon that would apply also to the lung tissue spill-over encountered above. If the tissue components have the same k_2, then there is a single exponential in the model response function (cf. Eq. 12). As a consequence MBF estimation methods based on K_1 will give no heterogeneity effects, whilst Iida's method, because it assumes a constant V_d, leads to a constant k_2 flow value independent of the actual weighted average rMBF value. However, apart from the lung partition coefficient (close to 0.1 ml/ml), it remains to be demonstrated that heterogeneity in regional V_d values do exist in the myocardium.

[^{11}C]methylglucose

The relative error is given in K_1 in [3] by a formula analogous to Eq. 8 above and the corresponding ε_1-function is given as a graph (Fig. 3 in reference [3]). Assuming a

decaying input function it follows that K_1 may be underestimated considerably in heterogeneous tissue if large differences in the transport rate constants occur, as for example at the border of an infarct. In normal tissue, assuming a 2:1 ratio for k_2 values between grey and white matter [34], the underestimation of K_1 may amount to 6%.

The variance of V_d is generally small [34] and therefore a close relation between K_1 and k_2 can be assumed. Using this fact and Eq. 29 and Fig. 5 in [3], the relative error for $V_d=K_1/k_2$ can be estimated to be <3% for a 2:1 ratio in k_2 between the components. However, the rather uniform distribution in V_d even in severe disease observed experimentally [34] indicates that the underestimation is probably smaller.

The results showed that, despite possible large underestimations in individual model rate constants, the error in the volume of distribution remained moderate. Since this parameter appears to be the most important one for [^{11}C]methylglucose, one may consider choosing an injection schedule for the tracer administration which minimizes the error in V_d due to tissue heterogeneity, if very accurate determinations of this parameter are needed. A constant input function should be optimal.

$CMRO_2$

If grey and white matter OEF were assumed to be the same, the error in the measured OEF due to tissue heterogeneity was always less than 5%, except for the situation where both grey and white matter CBF and V_d were reduced with normal OEF (=0.40), which resulted in a maximum overestimation of 15% in OEF.

Errors in OEF tended to be higher when grey (abnormal) and white (normal) matter OEFs were different. In this case the highest error (25%) was observed for increased grey matter CBF (1.6 ml/ml/min) with normal V_d (1.02 ml/ml) and reduced OEF (0.1). However, the error in OEF was always smaller than that in CBF (Fig. 1a). A substantial underestimation of OEF was observed in the tumor simulations [11].

Two tissue compartments

CMR_{glc} using FDG

Table 2 shows relative errors in the metabolic rate, which may be caused by tissue heterogeneity, for different parameter ratios $p_2^{(1)}/p_2^{(2)}$. The second column shows the range of heterogeneity of the two different tissues in the ROI where the values for the relative variance are largest. The assumption of a $p_2^{(1)}/p_2^{(2)}$. ratio equal to 2:1 for parameters $p_2=k_2+k_3$ is probably realistic from experience with rate constants observed in model fits to FDG uptake data in the brain. A ratio of 4:1 may occur only under extremely pathological conditions and a ratio of 10:1 can be considered completely unrealistic. Under such conditions both the approximations of the analytic method and the FDG model may no longer be valid. Therefore, tissue heterogeneity effects may lead to an overestimation of glucose metabolic rate using FDG of only a few percent under normal conditions and even in extreme cases the errors do not exceed the magnitude of methodological uncertainties of the FDG method as discussed in [35] and [36].

With $k_4=0$ the model expression for the FDG TAC is asymptotically linear in the accumulation rate [2] and the heterogeneity effects should become negligible with increasing measuring time. However, the assumption $k_4=0$ makes it necessary to restrict the measuring time to less than 60 min. Therefore, CMR_{glc} measured with the dynamic FDG method is still sensitive to tissue heterogeneity although, as the results show, the effects are rather small: less than 3% overestimation under normal conditions.

In regions with very high metabolism, like very active tumors, the crucial parameter k_2+k_3 never differs from normal values by more than a factor of 4 and, accordingly, the relative errors in CMR_{glc} are certainly smaller than 15%. It is in tissue with very low k_3, e.g. in infarcted tissue or in "cold" tumors, where large relative errors may occur. On the other hand, this implies a very low metabolic rate, so the absolute error remains small. Equation 8 shows that the absolute errors in the metabolic rate constant p_3 depend linearly on the average value of $p_1=K_1 \cdot k_2/(k_2+k_3)$, which is less sensitive to greatly reduced k_3 values.

The influence of tissue heterogeneity on FDG measurements has been investigated previously by others [37–39]. In contrast to the present study, the dependence of the fitted parameters on the degree of mixing was not investigated. Instead, the effect of using a two-tissue compartment model with and without k_4 on real data was investigated. In accordance with our conclusions concerning the kinetics of FESP (see below), the results indicated that the effect of tissue heterogeneity alone can give an apparent k_4. Further, these effects decreased with prolonged measuring time. This feature is also expected. If there is a pool that is effectively irreversible during the measuring times considered, the time course of the trac-

Table 2. Relative error in FDG metabolic rate for different ratios of parameter $p_2=k_2+k_3$ between two mixed tissues, (1) and (2)

$p_2^{(1)}/p_2^{(2)}$	Percent admixture of tissue 1 for maximal range of v^2	v^2	$\sigma p_3/p_3$
2:1	10–60	0.1	3%
4:1	10–40	0.5	15%
10:1	10	2	(60%, linear approx. no longer valid)

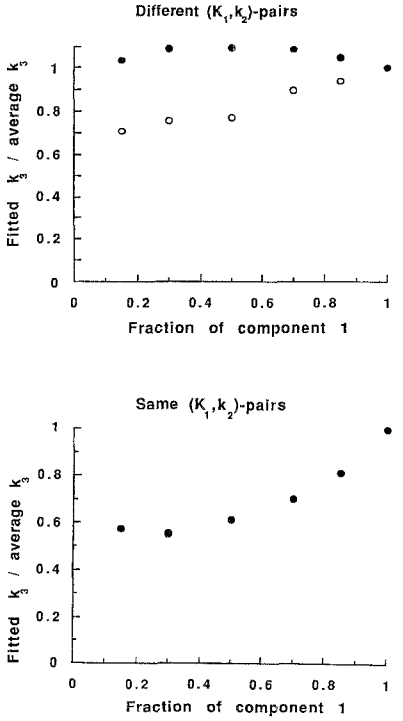

Fig. 4a, b. Change in $k_3=k_{on}\cdot B_{max}$ of FESP due to tissue heterogeneity. **a** (K_1, k_2) different for the two components. **b** (K_1, k_2) the same for the two components. In both plots $k_3=0$ for the second component (no specific binding). *Open circles*, k_4 included in the fit; *solid circles*, $k_4=0$ in the fit. With the same (K_1, k_2) for the two components (**b**) the fitted k_4 is less than 0.0003 for all mixings and the results almost coincide with the corresponding results using $k_4=0$

er will be asymptotically described by a simple model which is linear in two parameters [2]. The mixture of two (or more) TACs that are linear in the parameters is again linear (cf. Eqs. 3 and 4).

MAO-B

When grey and white matter only differ in K_1 and V_f (i.e. have the same k_2 and k_3), the resulting error in K_1 is less than 2% and negligible for all other parameters. The highest error in k_2 was obtained when k_2 was reduced to 0.06 min^{-1} with unchanged k_3 (0.25 min^{-1}). In this case the maximum error in k_2 was 36% with a maximum error in k_3 of 9%. The maximum error in k_3 went up to 23% if k_3 itself was also reduced to 0.1 min^{-1}. Interestingly, the maximum error in k_2 was reduced to 16% in this case.

Radioligand binding

Tracer doses: FESP

Results of the simulation calculations for FESP are shown in Fig. 4. The inclusion of the rate constant k_4 improved the fits only marginally in the case where specific and non-specific binding had identical rate constants K_1 and k_2 (Fig. 4b) and resulted in very small k_4 (less than 0.0003) and almost unchanged k_3. In the other case with a factor of 4 difference in K_1 between the two components (Fig. 4a) there were some improvements in the fits when k_4 was included and a quite large change in the k_3 value. In this case larger values of k_4 (0.0026 with 15% admixture of tissue void of receptors) were obtained.

The results show that errors in k_3 due to tissue heterogeneity caused by mixtures of tissue with specific and non-specific binding may be considerable. A 50%/50% mixture of specific and non-specific binding tissue with identical K_1 and k_2 rate constants leads to a 40% underestimation of k_3. With smaller values for K_1 and k_2 in tissue with non-specific binding the errors are somewhat smaller, but in this case the mixed TAC may simulate a non-existent k_4 rate constant. Depending on whether a rate constant k_4 is included or not, k_3 is over- or underestimated. These features of the two-tissue compartment model have been observed in experimental FDG data [37, 38].

Pharmacological doses: [^{11}C]Flumazenil

Of the binding parameters, B_{max} was the least sensitive to tissue heterogeneity (Fig. 5a). The small deviation of B_{max} from the average can be understood as follows. B_{max} is here assumed to be determined in a double experiment, one with a negligible amount of unlabelled ligand (high SA), and the other with a considerable amount of unlabelled ligand co-injected with the radioligand (low SA). Out of these experiments, the one with low SA is most important for the B_{max} estimate (cf. Scatchard plots). In this case the time course of the radioligand rapidly reaches a fairly constant level not far below the value $SA\cdot B_{max}$. For the determination of B_{max} the late part of the time course is more important than the early one, because only then is an appreciable amount of radioligand bound. A linear combination of two time courses, each with a plateau, results in a time course again with a plateau, and the new level is a linear combination of the original levels.

The small deviations of the B_{max} estimates from the average values are in sharp contrast to the considerable deviation from the expected average value of the parameter $k_{on}\cdot B_{max}=k_3$ obtained from simulations of the standard two-tissue compartment model applied to a single scan using tracer doses of FESP (see above). Also in the simulations of [^{11}C]flumazenil data, the product $k_{on}\cdot B_{max}=k_3$ show clear deviations from the expected average values.

In contrast to B_{max}, the fitted K_d value was found to deviate more and more from the true mean with decreasing fraction f_1 of the tissue with binding over a large range, $0.3<f_1<1$ (Fig. 5b). The figure shows that the fitted K_d was comparatively insensitive to the degree of mixing in this f_1 interval. K_d is the ratio between k_{off} and k_{on}, both of which also showed similar large deviations from the linear mixing. The sharp decrease in the fitted K_d value for f_1 below 0.3 can be observed experimentally. Parametric maps of K_d have a larger contrast between

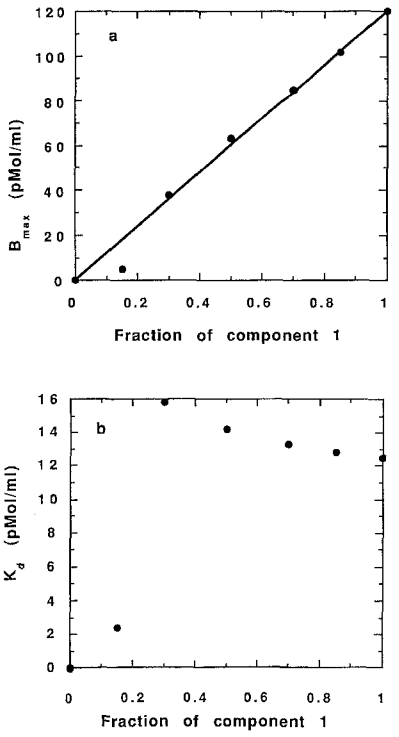

Fig. 5. Effects of tissue heterogeneity on (**a**) B_{max} and (**b**) K_d for [^{11}C]flumazenil. The following parameter settings were used in the simulations: $B_{max}^{(1)}$=120, $B_{max}^{(2)}$=0, $k_{on}^{(1)}$=0.004, $k_{on}^{(2)}$=0.0, $k_{off}^{(1)}$=0.05, $k_{off}^{(2)}$=0, $K_1^{(1)}$=0.4, $K_1^{(2)}$=0.10, $k_2^{(1)}$=0.50, $k_2^{(2)}$=0.15. A *straight line* has been fitted to the estimated B_{max} values

tissue with and tissue without binding than the corresponding maps of B_{max} [40]. When the two tissue components were assumed to have equal K_1 and k_2, the deviations from true mean values were somewhat smaller but the main pattern persisted: B_{max} was much less affected than K_d, k_{on} or k_{off}.

Physiologically, when tissue with receptors is mixed with receptor-free tissue, the density of receptors should decrease in proportion to the admixture of background tissue. Obviously this requirement is well fulfilled by the parameter B_{max} in the model. The affinity of receptors, on the other hand, should not be affected at all by admixture of receptor-free tissue. The results show that the parameter K_d roughly fulfills this requirement over a wide range of mixture fraction.

Conclusions

Depending on the complexity of the tracer model and the experimental protocol considered, either the analytical method or simulations were used. The latter method requires calculations by computer and is always time consuming, whereas the former can be used to obtain rapid information about tissue heterogeneity effects, at least in simple cases. However, the use of simulations gives more flexibility and they can be used in cases where the approximations of the analytic method are no longer valid. As previously mentioned, simulations are essential when no explicit solution can be obtained for the differential equations governing the time course of the tracer. Moreover, the method can be applied to problems not treated in this report. Examples are the combined effects of tissue heterogeneity and (a) random errors, (b) imperfect tracer model, (c) wrong input function and (d) tracer losses.

In conclusion, tissue heterogeneity can have a large effect on the estimation of physiological parameters. However, parameters such as CMR_{glc} and CBF, which enter linearly in the model expressions for the tissue radioactivity, are comparatively insensitive to heterogeneity under normal conditions, and other factors, such as noise, tracer losses and errors in the input function, can have more serious effects.

References

1. Phelps ME, Huang SC, Hoffman EJ, Kuhl DE. Validation of tomographic measurement of cerebral blood volume with C11-labeled carboxyhemoglobin. *J Nucl Med* 1979; 20: 328–334.
2. Patlak CS, Blasberg R, Fenstermacher J. Graphical evaluation of blood-to-brain transfer constants from multiple time uptake data. *J Cereb Blood Flow Metab* 1983; 3: 1–7.
3. Herholz K, Patlak CS. The influence of tissue heterogeneity on results of fitting nonlinear model equations to regional tracer uptake curves: with an application to compartmental models used in positron emission tomography. *J Cereb Blood Flow Metab* 1987; 7: 214–229.
4. Coxson PG, Salmeron EM, Huesman RH, Mazoyer BM. Simulation of compartmental models for kinetic data from a positron emission tomograph. *Comput Methods Programs Biomed* 1992; 37: 205–214.
5. Beck JV, Arnold KJ. Parameter estimation in engineering and science. New York: John Wiley, Chap. 7.
6. James F, Roos M. MINUIT. *Comput Phys Commun* 1975; 10: 343–367.
7. Frackowiak RSJ, Lenzi GL, Jones T, Heather JD. Quantitative measurement of regional cerebral blood flow and oxygen metabolism in man using ^{15}O and positron emission tomography: theory, procedure and normal values. *J Comput Assist Tomogr* 1980; 4: 727–736.
8. Koeppe RA, Holden JE, Ip WR. Performance comparison of parameter estimation techniques for the quantitation of local cerebral blood flow by dynamic positron computed tomography. *J Cereb Blood Flow Metab* 1985; 5: 224–234.
9. Ginsberg MD, Lockwood AH, Busto R, Finn RD, Butler CM, Cendan IE, Goddard J. A simplified in vivo autoradiographic strategy for the determination of regional cerebral blood flow by positron emission tomography: theoretical considerations and validation studies in the rat. *J Cereb Blood Flow Metab* 1982; 2: 89–98.
10. Raichle ME, Martin WRW, Herscovitch P, Mintun MA, Markham J. Brain blood flow measured with intravenous $H_2{}^{15}O$. II. Implementation and validation. *J Nucl Med* 1983; 24: 790–798.
11. Lammertsma AA, Jones T. Low oxygen extraction fraction in tumors measured with the oxygen-15 steady state technique: effect of tissue heterogeneity. *Br J Radiol* 1992; 65: 697–700.
12. Iida H, Kanno I, Takahashi A. Measurement of absolute myocardial blood flow with H_2O^{15} and dynamic positron emission tomography. Strategy for quantification in relation to the partial-volume effect. *Circulation* 1988; 78: 104–115.

13. Bergmann SR, Herrero P, Markham J. Noninvasive quantitation of myocardial blood flow in human subjects with oxygen-15-labeled water and positron emission tomography. *J Am Coll Cardiol* 1989; 14: 639–652.
14. Araujo LI, Lammertsma AA, Rhodes CG, McFalls EQ, Iida H, Rechavia E, Galassi A, De Silva R, Jones T, Maseri A. Noninvasive quantification of regional myocardial blood flow in coronary artery disease with oxygen-15-labeled carbon dioxide inhalation and positron emission tomography. *Circulation* 1991; 83: 875–885.
15. Lammertsma AA, De Silva R, Araujo LI, Jones T. Measurement of regional myocardial blood flow using $C^{15}O_2$ and positron emission tomography: comparison of tracer models. *Clin Phys Physiol Meas* 1992; 13: 1–20.
16. Lammertsma AA, Mazoyer BM. EEC concerted action on cellular degeneration and regeneration studied with PET: modelling expert meeting blood flow measurement with PET. *Eur J Nucl Med* 1990: 16: 807–812.
17. Mazoyer BM, Trebossen RT, Schoukroun C, Verrey B, Syrota A, Vacher J, Lemasson P, Monnet O, Bouvier A, Lecomte JL. Physical characteristics of TTV03, a new high spatial resolution time-of-flight positron tomograph. *IEEE Trans Nucl Sci* 1985; 37: 778–782.
18. Feinendegen LE, Herzog H, Wieler H, Patton DD, Schmid A. Glucose transport and utilization in the human brain: model using carbon-11 methyl glucose and positron emission tomography. *J Nucl Med* 1986; 27: 1867–1877.
19. Lammertsma AA, Jones T. Correction of the presence of intravascular oxygen-15 in the steady-state techniques for measuring regional oxygen extraction ratio in the brain. 1. Description of the method. *J Cereb Blood Flow Metab* 1983; 3: 416–424.
20. Phelps ME, Huang SC, Hoffman EJ, Selin C, Sokoloff L, Kuhl DE. Tomographic measurement of local cerebral glucose metabolic rate in humans with (F^{18})2-fluoro-2-deoxy-D-glucose: validation of method. *Ann Neurol* 1979; 6: 371–388.
21. Blomqvist G, Stone-Elander S, Halldin C, Roland P, Widén L, Lindqvist M, Swahn C-G, Långström B, Wiesel FA. Positron emission tomographic measurement of cerebral glucose utilization using [1-^{11}C]D-glucose. *J Cereb Blood Flow Metab* 1990; 10: 467–483.
22. Bahn MM, Huang SC, Hawkins RA, Satyamurthy N, Hoffman JM, Barrio JR, Mazziotta JC, Phelps ME. Models for in vivo kinetic interactions of dopamine D_2-receptors and 3-(2'-[^{18}F]fluoroethyl)spiperone examined with positron emission tomography. *J Cereb Blood Flow Metab* 1989; 9: 840–849.
23. Wienhard K, Coenen HH, Pawlik G, Rudolf J, Laufer P, Jovkar S, Stöcklin G, Heiss WD. PET studies of dopamine receptor distribution using [^{18}F]fluoroethylspiperone: findings in disorders related to dopaminergic system. *J Neural Transm Gen Sect* 1990; 81: 195–213.
24. Lammertsma AA, Bench CJ, Price GW, Cremer JE, Luthra SK, Turton D, Wood ND, Frackowiak RSJ. Measurement of cerebral monoamine oxidase B activity using L-[^{11}C]deprenyl and dynamic positron emission tomography. *J Cereb Blood Flow Metab* 1991; 11: 545–556.
25. Bustany P, Sargent T, Saudubray JM, Henry JF, Comar D. Regional human brain uptake and protein incorporation of [^{11}C]L-methionine studied in vivo with PET. *J Cereb Blood Flow Metab* (Suppl) 1981; 1: S17–S18.
26. Wienhard K, Herholz K, Coenen HH, Rudolf J, Kling P, Stöcklin G, Heiss WD. Increased amino acid transport into brain tumors measured by PET of L-(2-^{18}F)Fluorotyrosine. *J Nucl Med* 1991; 32: 1338–1346.
27. Huang SC, Barrio JR, Phelps ME. Neuroreceptor assay with positron emission tomography: equilibrium versus dynamic approaches. *J Cereb Blood Flow Metab* 1986; 6: 515–521.
28. Maziére B, Loc'h C, Baron JC, Sgouropoulos P, Duquesnoy N, D'Antona R, Cambon H. In vivo quantitative imaging of dopamine receptors in human brain using positron emission tomography and [^{86}Br]bromospiperone. *Eur J Pharmacol* 1985; 114: 267–272.
29. Arnett CD, Wold AP, Shiue CY, Fowler JS, McGregor RR, Christman DR, Smith MR. Improved delineation of human dopamine receptors using [^{18}F]-*N*-methylspiroperidol and PET. *J Nucl Med* 1986; 27: 1878–1882.
30. Wong DF, Gjedde A, Wagner HN Jr. Quantification of neuroreceptors in the living human brain. I. Irreversibvle binding of ligands. *J Cereb Blood Flow Metab* 1986; 6: 137–146.
31. Barrio JR, Satyamurthy N, Huang SC, Keen RE, Nissenson CHK, Hoffman JM, Ackerman RF, Bahn MM, Mazziotta JC, Phelps ME. 3-(2'-[^{18}F]fluoroethyl)spiperone: in vivo biochemical and kinetic characterization in rodents, nonhuman primates, and humans. *J Cereb Blood Flow Metab* 1989; 9: 830–839.
32. Farde L, Hall H, Ehrin H, Sedvall G. Quantitative analysis of D_2 dopamine receptor binding in the living human brain by PET. *Science* 1986; 231: 258–261.
33. Lammertsma AA, Cunningham VJ, Deiber MP, Hether JD, Bloomfield PM, Nutt J, Frackowiak RSJ, Jones T. Combination of dynamic and integral methods for generating reproducible functional CBF images. *J Cereb Blood Flow Metab* 1990; 10: 675–686.
34. Gjedde A, Wienhard K, Heiss WD, Kloster G, Diemer NH, Herholz K, Pawlik G. Comparative regional analysis of 2-fluorodeoxyglucose and methylglucose uptake in brain of four stroke patients. With special reference to the regional estimation of the lumped constant. *J Cereb Blood Flow Metab* 1985; 5: 163–178.
35. Wienhard K, Pawlik G, Herholz K, Wagner R, Heiss WD. Estimation of local cerebral glucose utilization by positron emission tomography of [^{18}F]2-fluoro-2-deoxy-D-glucose: a critical appraisal of optimization procedures. *J Cereb Blood Flow Metab* 1985; 5: 115–125.
36. Lammertsma AA, Brooks DJ, Frackowiak RSJ, Beaney RP, Herold S, Heather JD, Palmer AJ, Jones T. Measurement of glucose utilization with [^{18}F]2-fluoro-2-deoxy-D-glucose: a comparison of different analytical methods. *J Cereb Blood Flow Metab* 1987; 7: 161–172.
37. Schmidt K, Mies G, Sokoloff L. Model of kinetic behavior of deoxyglucose in heterogeneous tissues in brain: a reinterpretation of the significance of parameters fitted to homogeneous tissue. models. *J Cereb Blood Flow Metab* 1991; 11: 10–24.
38. Schmidt K, Lucignani G, Moresco RM, Rizzo G, Gilardi MC, Messa C, Colombo F, Fazio F, Sokoloff L. Errors introduced by tissue heterogeneity in estimation of local cerebral glucose utilization with current kinetic models of the [^{18}F]fluorodeoxyglucose method. *J Cereb Blood Flow Metab* 1992; 12: 823–824.
39. Lucignani G, Schmidt KC, Moresco RM, Striano G, Colombo F, Sokoloff L, Fazio F. Measurement of regional cerebral glucose utilization with fluorine-18-FDG in PET in heterogeneous tissues: theoretical considerations and practical procedure. *J Nucl Med* 1993; 34: 360–369.
40. Blomqvist G, Pauli S, Farde L, Eriksson L, Persson A, Halldin C. Maps of receptor binding parameters in the human brain – a kinetic analysis of PET measurements. *Eur J Nucl Med* 1990; 16: 257–265.